Electronic Supplementary Information for

Engineering Donor-Acceptor Conjugated Polymers for High-Performance and Fast-Response Organic Electrochemical Transistors

Hanyu Jia,[a,d†] Zhen Huang,[b†] Peiyun Li,[a†] Song Zhang,[c] Yunfei Wang,[c] Jie-Yu Wang,[b] Xiaodan Gu,[c] and Ting Lei[a,e*]

a Key Laboratory of Polymer Chemistry and Physics of Ministry of Education, School of Materials Science and Engineering, Peking University, Beijing 100871, China.

b College of Chemistry and Molecular Engineering, Peking University, Beijing 100871, China.

c School of Polymer Science and Engineering, The University of Southern Mississippi, Hattiesburg, MS 39406, USA.

d School of Materials Science and Engineering, The Key Laboratory of Material Processing and Mold of Ministry of Education, Henan Key Laboratory of Advanced Nylon Materials and Application, Zhengzhou University, Zhengzhou 450001 China

e Beijing Key Laboratory for Magnetoelectric Materials and Devices, Peking University, Beijing 100871, China.

†These authors contributed equally to this work.

*Correspondence and requests for materials should be addressed to T.L. (tinglei@pku.edu.cn).

Table of Contents

1. Experimental Details

Materials

All chemical reagents were purchased and used as received unless otherwise indicated. All air and water sensitive reactions were performed under nitrogen atmosphere. Dichloromethane (DCM), tetrahydrofuran (THF), toluene, and *N,N*-dimethylformamide (DMF) were dried by a JC Meyer solvent drying system.

Chemical Structure and Optoelectronic Property Characterization

^{1}H NMR and ^{13}C NMR spectra were recorded on Bruker ARX-400 (400 MHz), Bruker AVANCE III (500 MHz), and Bruker 600M (600 MHz). All chemical shifts were reported in parts per million (ppm). ^{1}H NMR chemical shifts were referenced to $CDCl_3$ (7.262 ppm) and $CDCl_2CDCl_2$ (5.984 ppm), ^{13}C NMR chemical shifts were referenced to $CDCl_3$ (77.00 ppm). Mass spectra were recorded on an AB Sciex-5800 MALDI-TOF mass spectrometer and a Bruker Solarix XR mass spectrometer. Elemental analyses were performed on Vario EL elemental analyzer. Thermal gravity analyses (TGA) were carried out on a TA Instrument Q600 SDT analyzer. Absorption spectra were recorded on PerkinElmer Lambda 750 UV-Vis spectrometer. Cyclic voltammograms were measured through an electrochemical workstation SP-300 (BioLogic Science Instruments). A standard three-electrode setup was established with employing polymer-coated ITO glass slides as the working electrode (WE), a block of platinum mesh as the counter electrode (CE), and an Ag/AgCl pellet (Warner Instruments) as the reference electrode (RE), further calibrated against ferrocene (Fc/Fc^+). The measurements were carried out in aqueous solution with 0.1 M NaCl or in acetonitrile with 0.1 M tetrabutylammonium hexafluorophosphate as the supporting electrolyte with a scan rate of 50 mV/s. Ionization potentials and electron affinity were obtained using the equation: IP = ($E_{Ox} - E_{Fc/Fc^+} + 4.8$) eV, EA = ($E_{Red} - E_{Fc/Fc^+} + 4.8$) eV. The geometries and frontier orbitals of bgDPP-T, bgDPP-T2, lgDPP-MeOT2, and bgDPP-MeOT2 trimers were calculated at the B3LYP/6-311G(d,p) level using Gaussian 16 software package.

Size Exclusion Chromatography Measurement

Polymer number-average molecular weight (M_n) and molecular weight distributions ($Đ = M_w/M_n$) were measured by size exclusion chromatography (SEC). Chloroform SEC analyses were performed on a Waters 1515 instrument equipped with a PLMIXED 7.5×50 mm guard column and two PLMIXED-C 7.5×300

columns and a differential refractive index detector using chloroform as the eluent at 35℃ with a flow rate of 1 mL min^{-1}. The instrument was calibrated with 10 PS standards, and chromatograms were processed with Waters Breeze software. Hexafluoroisopropanol SEC analyses were performed on a Waters 1515 instrument equipped with a PLMIXED 7.5×50 mm guard column and two PLMIXED-C 7.5×300 columns and a differential refractive index detector using hexafluoroisopropanol as the eluent at 35 ℃ with a flow rate of 1 mL min^{-1}. The instrument was calibrated with 10 PMMA standards, and chromatograms were processed with Waters Breeze software.

AFM and GIWAXS characterization

Atomic Force Microscopy (AFM) measurements were performed with a Cypher atomic force microscope (Asylum Research, Oxford Instruments). The surface morphology was recorded with a scan rate of 2-3 Hz at AC mode. GIWAXS experiment was performed on Xenocs Xuess 2.0 beamline, with an incident X-ray angle of 0.2 degrees and wavelength of 1.54 angstrom. The scattered signal is collected by Pilatus 1M detector at a sample to detector distance of 150 mm. Data processing is performed in Igor Pro software with Nika and WAXTools packages.

Spectroelectrochemistry

Spectroelectrochemistry was performed with an ITO-coated glass slide, spun cast with the polymer solution ($3*10^{-3}$ M chloroform solution) at the rotating speed of 500 rpm for 45 s without any additional processing. These polymer-coated ITO slides were employed as the WE and immersed into the cuvette filled with 0.1 M aqueous NaCl solution, following with the use of Pt mesh (CE) and Ag/AgCl pellet (RE). A PerkinElmer Lambda 750 UV-vis spectrometer was used with the beam path passing through the electrolyte-filled cuvette and polymer-coated ITO samples. A background spectrum with cuvette/electrolyte/ITO was recorded before a potential was applied to the cell. The potential was applied to the WE for 5 s before the spectra were recorded and lasted for a certain amount of time until the completion of spectrum scanning.

OECT Fabrication and Characterization

The OECTs fabrication included the deposition and patterning of the metallic electrodes, parylene layer, and polymer in the channel. In detail, the silica substrates were thoroughly cleaned by sonication in acetone, DI

water, and isopropyl alcohol, followed by nitrogen blow drying and brief oxygen plasma cleaning. Metal pads, interconnects, and source/drain contacts (defining the channel length and width) were patterned by a lift-off process. 5 nm of chromium and 50 nm of gold were subsequently deposited using a metal evaporator, and metal lift-off was carried out in acetone. Metal interconnects and pads were insulated by depositing 2 μm of parylene-C using a PDS 2010 Labcoater-2, with a 3-(trimethoxysilyl)propyl methacrylate (A-174 Silane) adhesion promoter. A 2% aqueous solution of industrial cleaner (Micro-90) was subsequently spun coated to act as an anti-adhesive for a second, sacrificial 2 μm parylene-C film, which was used to simultaneously define the active channel area, and to pattern the underlying parylene layer. Samples were subsequently patterned with a 5 μm thick layer of AZ9260 photoresist and AZ-400K developer. The patterned areas were opened by reactive ion etching with O_2 plasma using an LCCP-6A reactive ion etcher (Leuven Instruments). For the polymer film formation in the opened channels, the polymer solution was spun cast on the etched devices with different rotating speeds depending on the desired film thickness. After a peeling-off process of the second sacrificial parylene layer, the OECTs were ready for measurement. The device characterization was performed on the Keithley 4200 SCS. Ag/AgCl pellet (Warner Instruments) was employed as the gate and immersed into a 0.1 M NaCl solution, which covers the polymer film in the channel. During the on-off switching test, the V_{DS} was set as -0.4V, the Ag/AgCl pellet gate was applied with -0.4 V for 2 sec and then switched off for 2 sec, and the sampling speed was fixed as 1 Hz.

Electrochemical Impedance Spectra

Electrochemical impedance spectra (EIS) were performed on the polymer-coated electrodes using the electrochemical workstation SP-300 (BioLogic Science Instruments). Polymer film covered on the electrodes were patterned as squares with certain areas through lithography technique. These polymer-coated electrodes with glass substrate were employed as the working electrode and fully covered with a 0.1 M NaCl solution, followed with the employment of Pt mesh (CE) and Ag/AgCl pellet (RE) to establish a standard three electrodes system. The capacitances of polymers on electrodes with various sizes were obtained through the potentio-EIS method, with setting the DC offset voltage as the maximum achievable doping for each polymer. The AC amplitude of voltage in the form of sine-wave on the WE was set as 10 mV (RMS) and the frequency was scanned from 100 kHz to 1 Hz. The as-obtained Bode plots or Nyquist plots were fitted to an equivalent circuit, namely the Randle's circuit $R_s(R_p||C)$, via the software EC-Lab view. The thickness of the

films was determined in the dry state with a DEKTAK profilometer (Bruker).

2. Table S1-S4 and Figure S1-S23

Table S1. Summary of Synthetic Conditions and Molecular Weights of the DPP Polymers.

Polymer	Catalyst/ligand	Cocatalyst	Yield [%]	M_n[a]	PDI[a]	M_n[b]	PDI[b]
P(lg3DPP-T)	$Pd_2(dba)_3$/P(*o*-tolyl)$_3$	/	20[c]	/	/	/	/
P(bgDPP-T)	$Pd(PPh_3)_4$	CuI	62	69.0	2.32	29.5	2.50
P(bgDPP-T2)	Pd $(PPh_3)_2Cl_2$	CuI	79	70.6	2.27	26.1	2.48
P(bgDPP-MeOT2)	$Pd(PPh_3)_2Cl_2$	CuI	84	61.7	2.37	30.1	2.62
P(lgDPP-MeOT2)	$Pd(PPh_3)_2Cl_2$	CuI	26[c]	64.9	2.13	29.9	2.39

[a] Using chloroform as the eluent. [b] Using HFIP as the eluent. [c] Low yield because most of the polymers is insoluble.

Table S2. Optical and Electrochemical Properties of the DPP Polymers.

Polymer	E_{onset}[a] [V]	IP[a] [eV]	EA[a] [eV]	E_{onset}[b] [V]	HOMO[c] [eV]	$E_{g,DFT}$[c] [eV]	$E_{g,Opt}$[d] [eV]	λ_{onset}[d] [nm]
P(bgDPP-T)	0.55	4.98	3.69	0.58	–4.93	1.69	1.37	906
P(bgDPP-T2)	0.48	4.91	3.74	0.40	–4.92	1.74	1.42	875
P(bgDPP-MeOT2)	0.19	4.62	3.72	0.23	–4.53	1.50	1.17	1062
P(lgDPP-MeOT2)	–0.08	4.35	3.75	0.02	–4.53	1.50	1.07	1163

[a] Determined by the CV of the polymer film on ITO coated glass substrates in acetonitrile with 0.1 M [*n*-Bu_4N][PF_6] as the supporting electrolyte. [b] 0.1 M NaCl aqueous solution as the supporting electrolyte. [c] Calculated results at the B3LYP/6-311G(d,p) level. [d] Obtained from the UV-Vis-NIR absorption spectra.

Table S3. Comparison of the OECT Performances for Polythiophene and D-A Type Polymers.

Polymer	D-A polymer Y(es)/N(o)	μ [$cm^2\ V^{-1}\ s^{-1}$]	C^* [$F\ cm^{-3}$]	μC^* [$F\ cm^{-1}\ V^{-1}\ s^{-1}$]	τ_{on} [ms]	τ_{off} [ms]	Reference
P(g2T-T)	N	0.28±0.10	220±30	135±9	1.4[a]	1.4[a]	[2,3]
P(g2T-TT)	N	0.94±0.25	297	261±29	0.42[a]	0.043[a]	[4,5]
p(g2T2-g4T2)	N	1.72±0.31	187±8	522	N/A[e]	N/A[e]	[6]
PEDOT: PSS	N	1.9±1.3	39±3	47±6	N/A[e]	0.102[a]	[7]
PTHS+EG	N	$1.3±1.1\times10^{-3}$	124±38	5.5±0.1	0.4[b]	N/A[e]	[8,9]
PIBET-AO	Y	N/A[e]	N/A[e]	5.4[f]	590[c]	390[c]	[10]
BBL	Y	7×10^{-4}	930±40	0.65±0.028[g]	900[c]	200[c]	[11]
CPEK	Y	5×10^{-3}[h]	134	0.67[f]	N/A[e]	0.137[d]	[12]
P(gPyDPP-MeOT2)	Y	0.030±0.007	60	1.8±0.42[g]	0.77[a]	0.46[a]	[13]
P(bgDPP-MeOT2)	Y	1.63±0.14[h]	120.0±2.4	195±21	0.516[a]	0.030[a]	This work
P(lgDPP-MeOT2)	Y	2.15±0.27[h]	80.8±1.4	174±25	0.578[a]	0.063[a]	This work

Time constant measurements were performed with channel geometries (*W*/*L*) of [a] 100/10 μm, [b] 5/10 μm, [c] 390000/20 μm, and [d] 1000/40 μm. [e] Data not available in the reference. [f] μC^* was estimated based on the

given transconductance and device geometries. [g] μC^* was calculated as the product of the measured μ and C^*. [h] μ was calculated from the measured μC^* and C^*.

Table S4. **Summary of OECT Performances of Other Polymers Processed with CF and HFIP.**

Polymer	Solvant	μC^* [F cm^{-1} V^{-1} s^{-1}]
P(lgDPP-T)	HFIP	10±2
P(lgDPP-T2)	HFIP	36±17
P(g2T-T)	CF	72±8
P(g2T-T)	HFIP	97±8

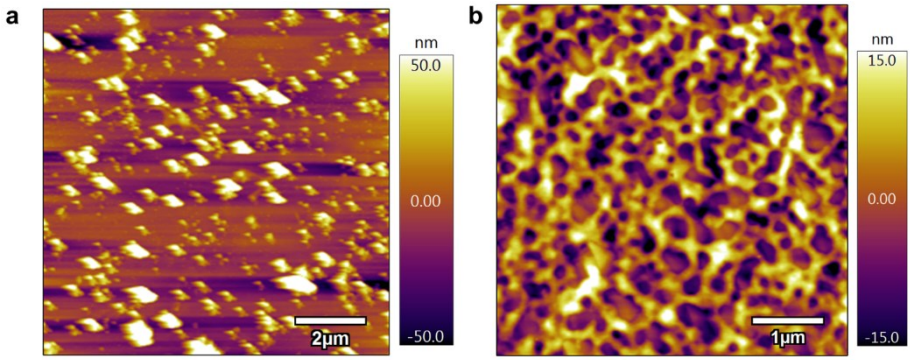

Figure S1 AFM topography images of the as-fabricated P(bgDPP-MeOT2) film. The polymer channel was fabricated by spin-coating its 3 mg/mL (a) chloroform and (b) hexafluoroisopropanol solution at 1000 rpm for 60 s on a silicon dioxide substrate.

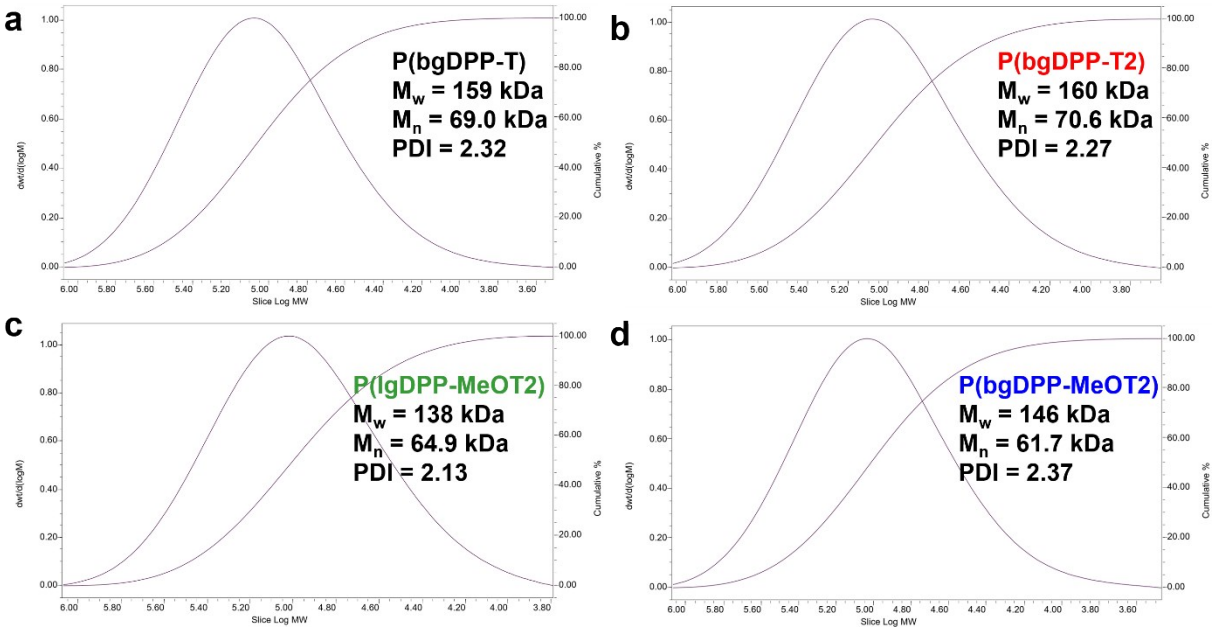

Figure S2 Molecular weights and polymer dispersity index (PDI) of (a) P(bgDPP-T), (b) P(bgDPP-T2), (c) P(lgDPP-MeOT2), and (d) P(bgDPP-MeOT2) measured by GPC with $CHCl_3$ as the eluent.

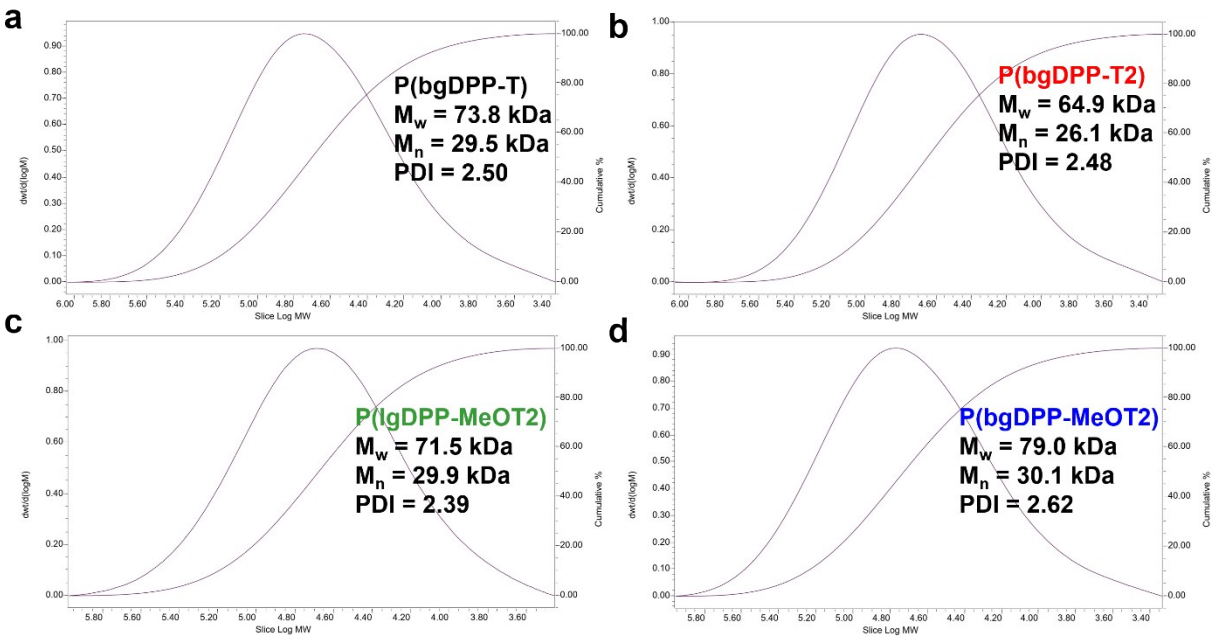

Figure S3 Molecular weights and polymer dispersity index (PDI) of (a) P(bgDPP-T), (b) P(bgDPP-T2), (c) P(lgDPP-MeOT2), and (d) P(bgDPP-MeOT2) measured by GPC with HFIP as the eluent.

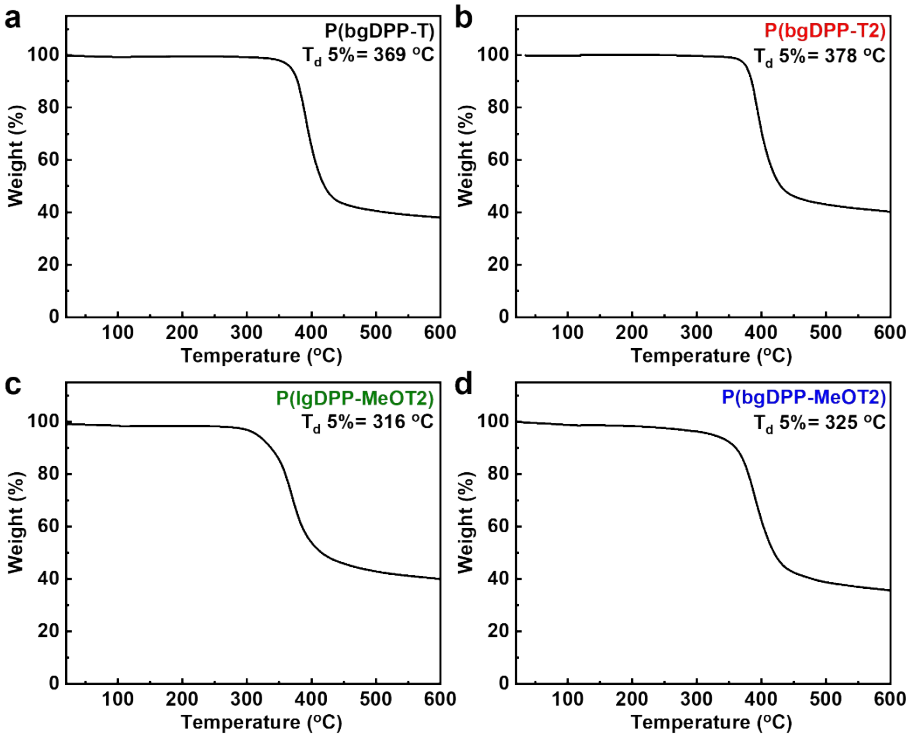

Figure S4 Thermal gravity analyses (TGA) of (a) P(bgDPP-T), (b) P(bgDPP-T2), (c) P(lgDPP-MeOT2), and (d) P(bgDPP-MeOT2).

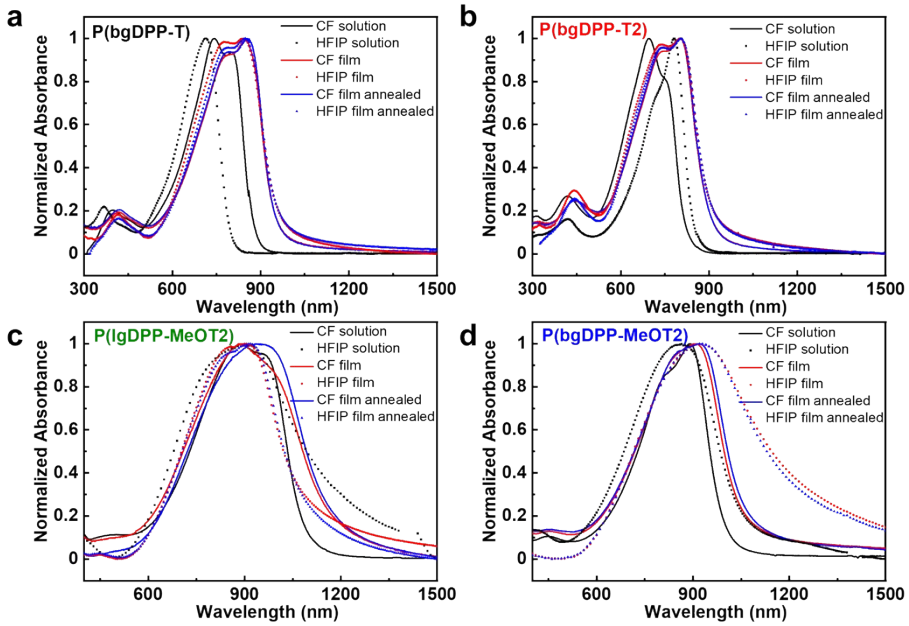

Figure S5 Normalized UV-vis-NIR absorption spectra of (a) P(bgDPP-T), (b) P(bgDPP-T2), (c) P(lgDPP-MeOT2) and (d) P(bgDPP-MeOT2) with processing solvent of chloroform (CF) and hexafluoroisopropanol (HFIP).in solution, in thin film, and in annealed thin film (80 ^{o}C, 10 min).

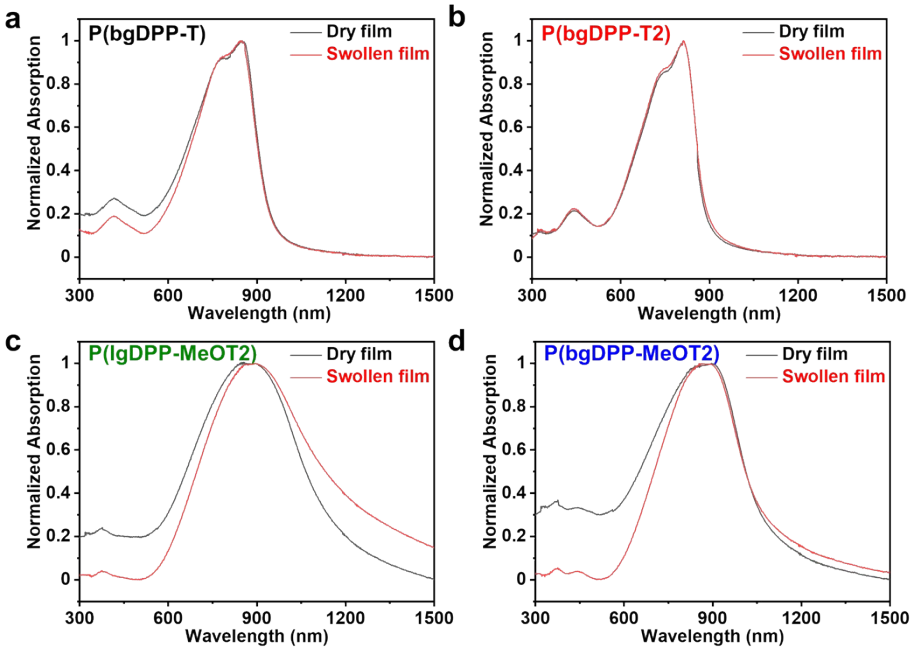

Figure S6. UV-Vis spectra of the four DPP polymer films in the dry and swollen state. (a) P(bgDPP-T), (b) P(bgDPP-T2), (c) P(lgDPP-MeOT2), (d) P(bgDPP-MeOT2).

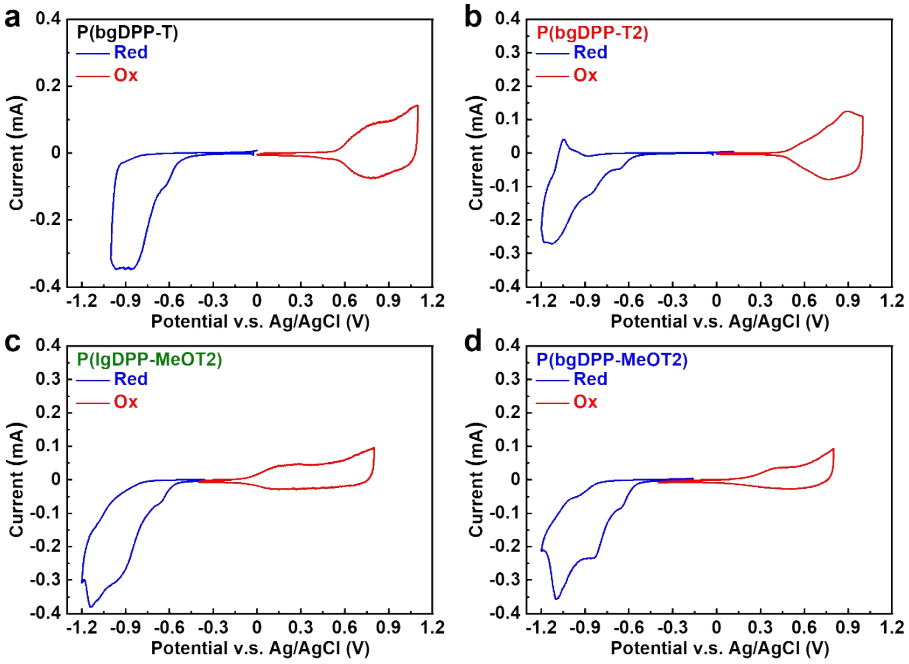

Figure S7 Cyclic voltammograms of (a) P(bgDPP-T), (b) P(bgDPP-T2), (c) P(lgDPP-MeOT2), and (d) P(bgDPP-MeOT2) in acetonitrile solution with 0.1 M tetrabutylammonium hexafluorophosphate as the supporting electrolyte.

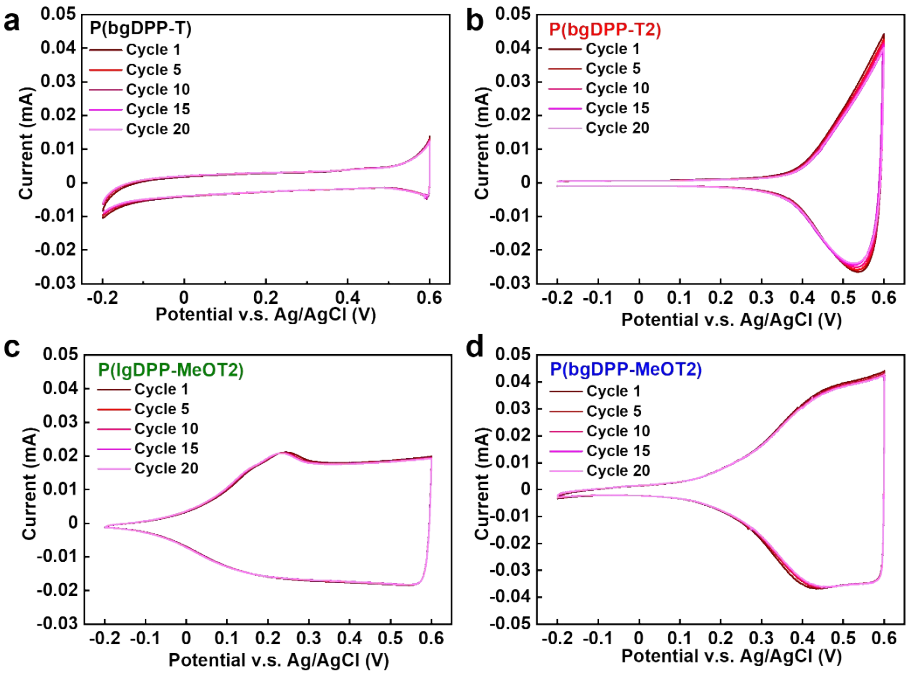

Figure S8 Cyclic voltammograms of (a) P(bgDPP-T), (b) P(bgDPP-T2), (c) P(lgDPP-MeOT2), and (d) P(bgDPP-MeOT2) in aqueous solution with 0.1 M sodium chloride as the supporting electrolyte. All the CV scans were repeated for 20 cycles.

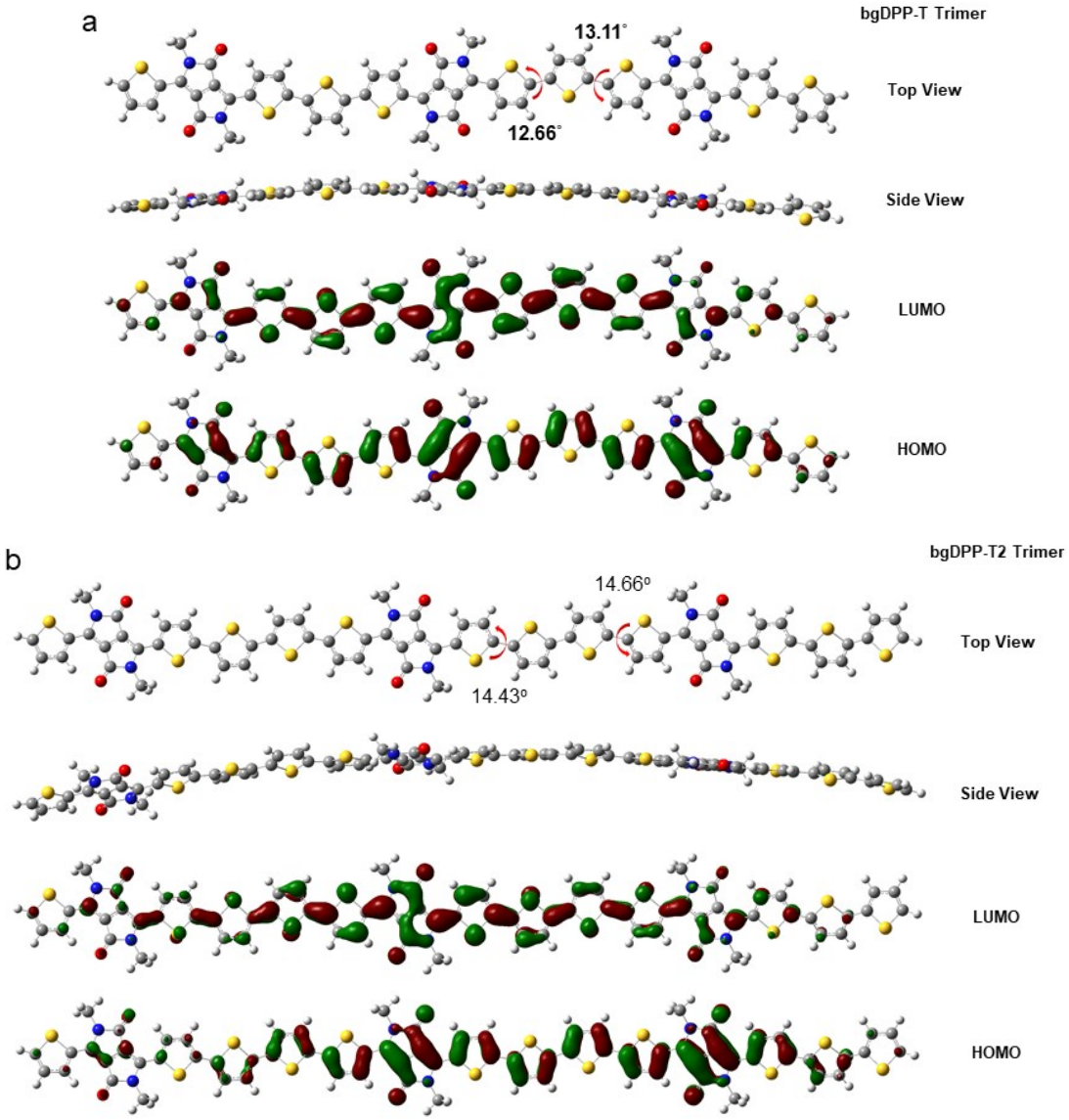

Figure S9 DFT-optimized geometries and molecular frontier orbitals of the trimer of (a) bgDPP-T and (b) bgDPP-T2. Calculations were performed at B3LYP/6-311G(d,p) level. Branched glycol side chains were replaced with methyl groups to simplify the calculation.

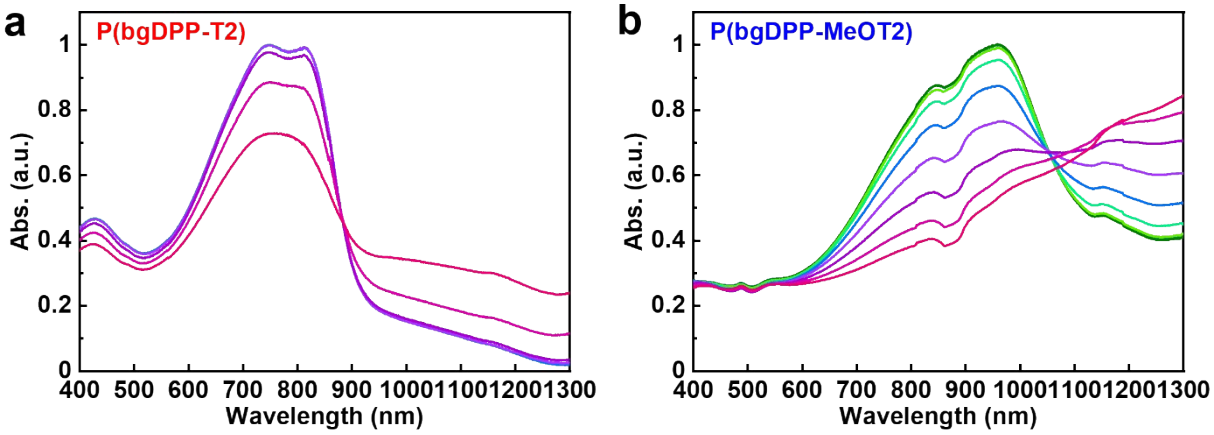

Figure S10 UV-vis-NIR spectra of (a) P(bgDPP-T) and (b) P(bgDPP-T2) upon continuously increasing the bias on the polymer film. The applied voltage ranged from −0.2 V to 0.6 V with an interval of 0.1 V.

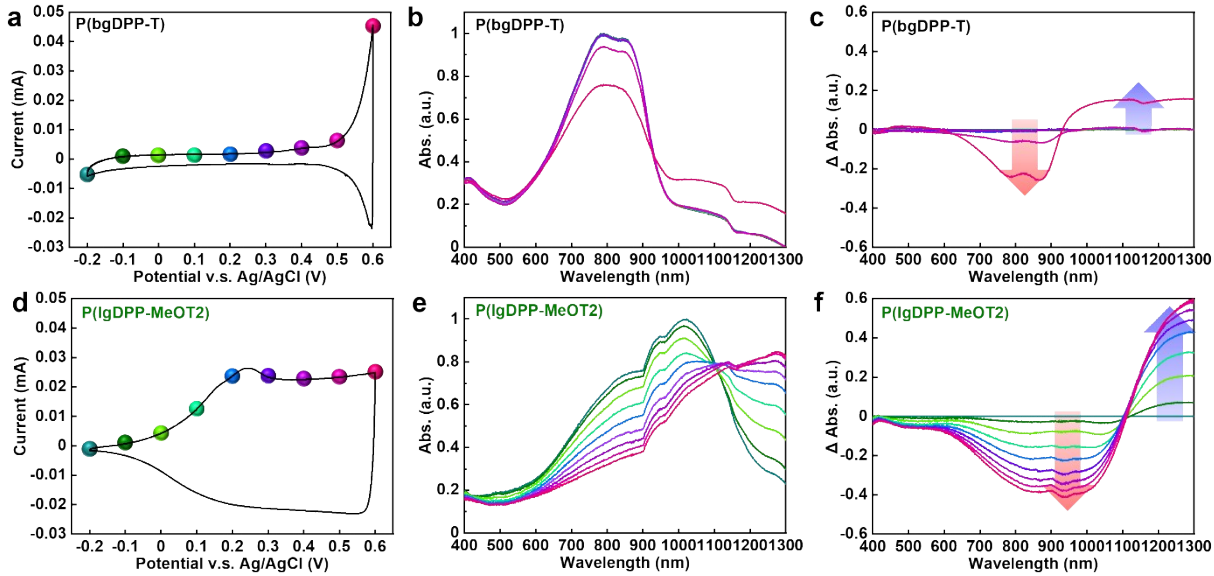

Figure S11 Cyclic voltammograms, UV-vis-NIR spectra, and the differential spectra of (a-c)P(bgDPP-T), and (d-f) P(lgDPP-MeOT2). The color-coding UV-vis-NIR spectra indicate the applied voltage on the polymer film, ranging from −0.2 V to 0.6 V with an interval of 0.1 V.

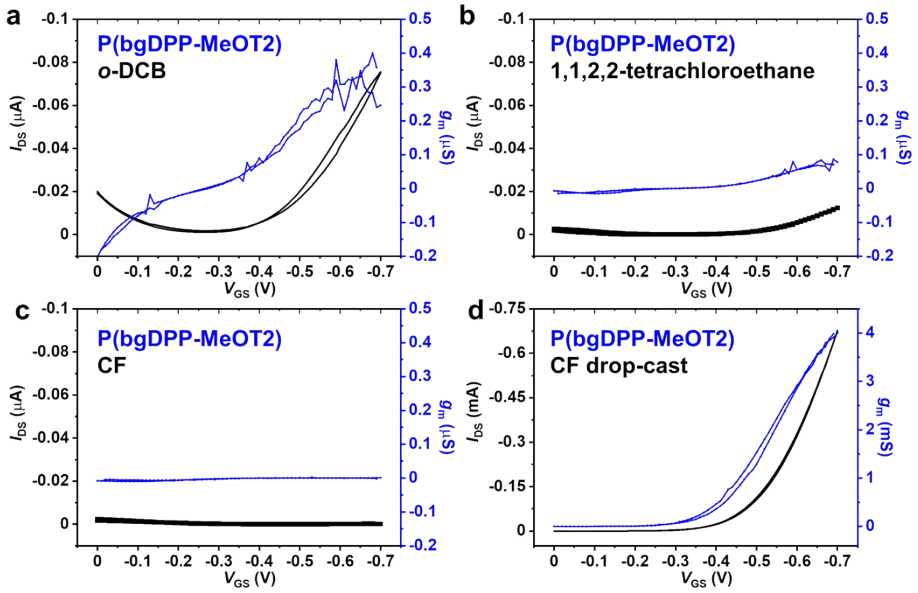

Figure S12 (a-c) OECT performance of P(bgDPP-MeOT2) with processed by o-DCB, TCE, and CF. All polymer solution was obtained with a concentration of 3 mg/mL, and spin-casting with a rotating speed of 1000 rpm. (d) OECT performance of P(bgDPP-MeOT2) with processed by CF. Channel film was obtained by drop cast 3 mg/mL CF solution. W/L = 100-10 μm for all polymer channels.

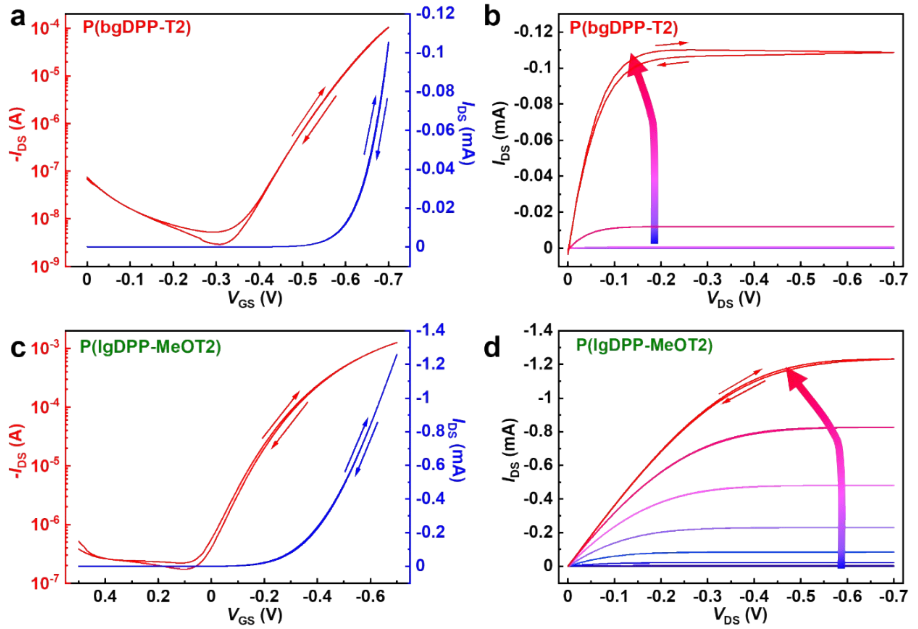

Figure S13 Transfer and output characteristics of (a-b) P(bgDPP-T2) and (c-d) P(lgDPP-MeOT2) OECTs. Channel dimensions: W/L = 1000/10 μm, d = 30.8±1.7 nm for P(bgDPP-T2), and 31.0±1.3 nm for P(lgDPP-MeOT2). V_{DS} was set to −0.6 V.

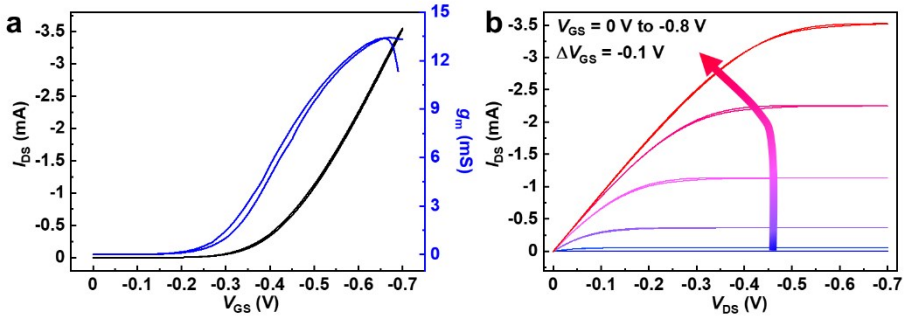

Figure S14 (a) Transfer and transconductance characteristics of P(bgDPP-MeOT2)-based OECT with a thick film, (b) The corresponding output characteristics. Channel dimensions: W/L = 1000/10 μm, d = 75.0±2.0 nm. V_{DS} was set to −0.6 V.

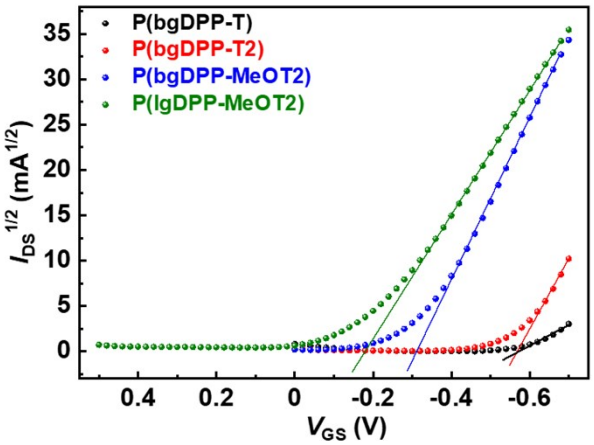

Figure S15 $I_{DS}^{1/2}$ *vs*. V_{GS} plots of the DPP polymer based OECTs. The threshold voltages, V_{Th}, were determined by extrapolating the linear region of the curves. Channel dimensions: W/L = 1000-10 μm, d = 29.0±0.8 nm for P(bgDPP-T), 30.8±1.7 nm for P(bgDPP-T2), 35.2±1.7 nm for P(bgDPP-MeOT2), and 31.0±1.3 nm for P(lgDPP-MeOT2). V_{DS} was set to −0.6 V.

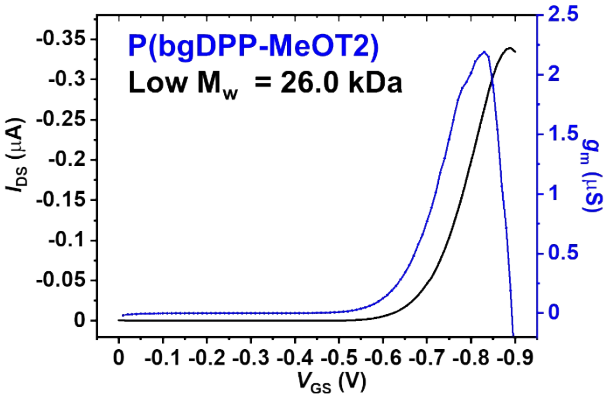

Figure S16 OECT performance of low M_w P(bgDPP-MeOT2), using chloroform as the eluent of GPC, PDI = 1.69. Polymer solution (HFIP) was obtained with a concentration of 3 mg/ mL, and spin-cast with a rotating speed of 1000 rpm. The channel thickness was measured as 65.2±5.6 nm. W/L = 100-10 μm. The ultra-low gm shows that molecular weight has a great influence on device performance.

To confirm the universality of HFIP, we synthesized polythiophene with glycol side chain, namely P(g2T-T), to investigate the influence led by the processing solvent of HFIP. As shown in Figure S17, we found that the solvent of CF exhibits better solubility of P(g2T-T) than HFIP, whereas after stirring overnight (16 h), P(g2T-T) is also fully dissolved in HFIP. Afterward, we measured the OECT performance of P(g2T-T) channel processed with CF and HFIP. OECT devices based on P(g2T-T) with processed by CF solution or HFIP solution both exhibit good OECT performance. Clearly, under the same channel geometry, OECTs using HFIP as the processing solvent achieve higher μC* of 97±8 $F \cdot cm^{-1} \cdot V^{-1} \cdot s^{-1}$ than that using CF (72±8 $F \cdot cm^{-1} \cdot V^{-1} \cdot s^{-1}$), which is quite consistent with the reported results of 62±24 $F \cdot cm^{-1} \cdot V^{-1} \cdot s^{-1}$.[9] Therefore, we consider the processing solvent of HFIP probably exhibits huge potential in both D-A conjugated polymers and polythiophenes for OECT applications.

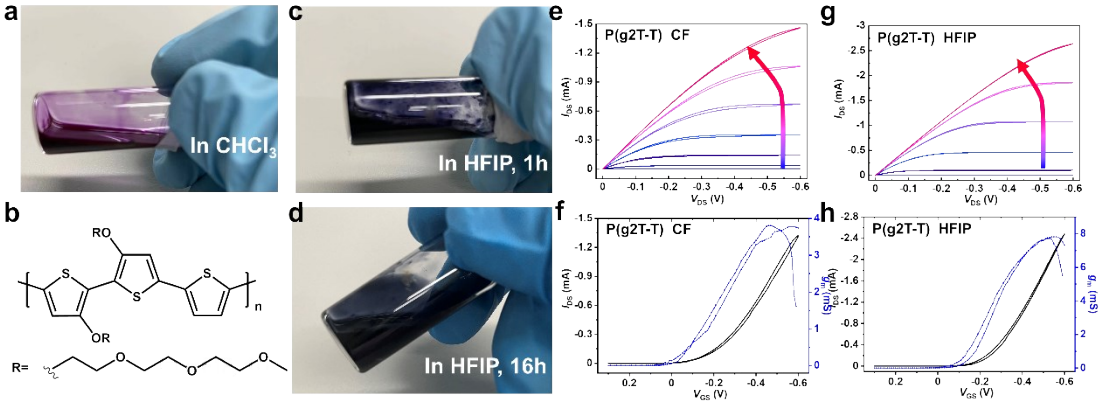

Figure S17 Dissolution behaviors and OECT performance of P(g2T-T) in solvents of chloroform (CF) and hexafluoroisopropanol (HFIP). (a) P(g2T-T) fully dissolved in CF in 1h. (b) The chemical structure of P(g2T-T). (c) P(g2T-T) partially dissolved in HFIP after stirring for 1h. (d) P(g2T-T) fully dissolved in HFIP after stirring for 16h. All polymer solution was obtained with a concentration of 3 mg/mL. The output curves (e, g) and transfer curves (f, h) of OECT devices with P(g2T-T) channel processed by CF and HFIP. All polymer solution was obtained with a concentration of 3 mg/ mL, and spin-casting with a rotating speed of 1000 rpm. The channel thickness was measured as 102.7±9.6 nm for CF solution and 174.0±26.3 nm for HFIP solution. W/L = 100-10 μm for all OECTs.

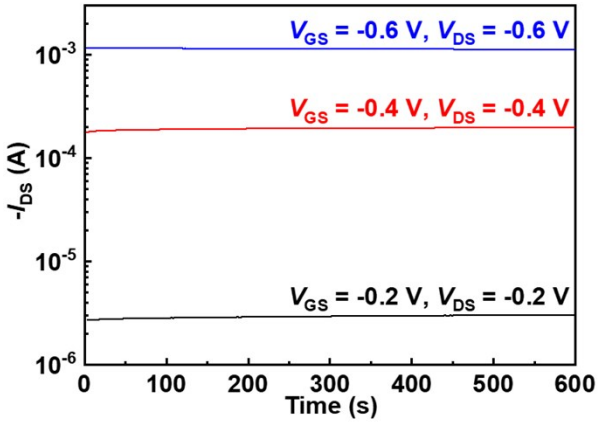

Figure S18 Continuous stressing of a P(bgDPP-MeOT2) OECT device upon the indicated V_{DS} and V_{GS} values.

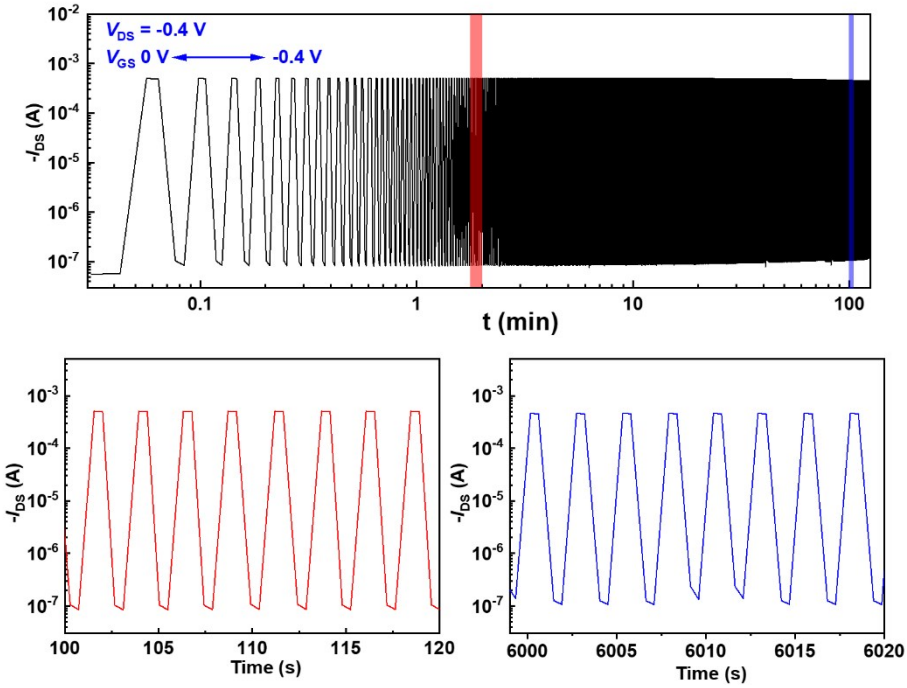

Figure S19 The enlargement view of the on-off switching plot of P(bgDPP-MeOT2) OECT device at two different time zones, highlighted with red and blue boxes. Switching on time of V_{GS} and the interval time were set as 2 s both, and the sampling speed was fixed as 1 Hz.

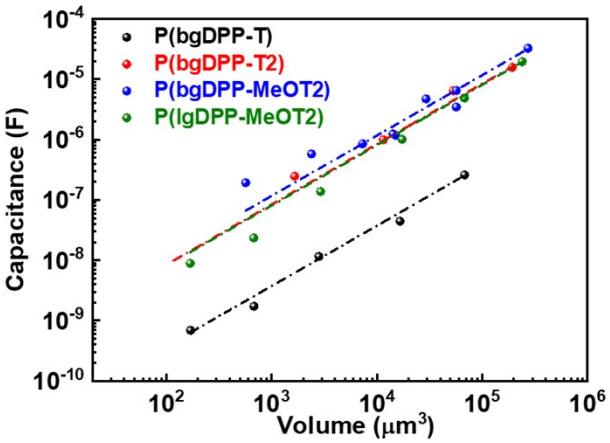

Figure S20 Capacitance-volume relationship of the DPP polymers. All the data were measured through the electrochemical impedance spectroscopy method. Linear fitting was performed to obtain their corresponding volumetric capacitance.

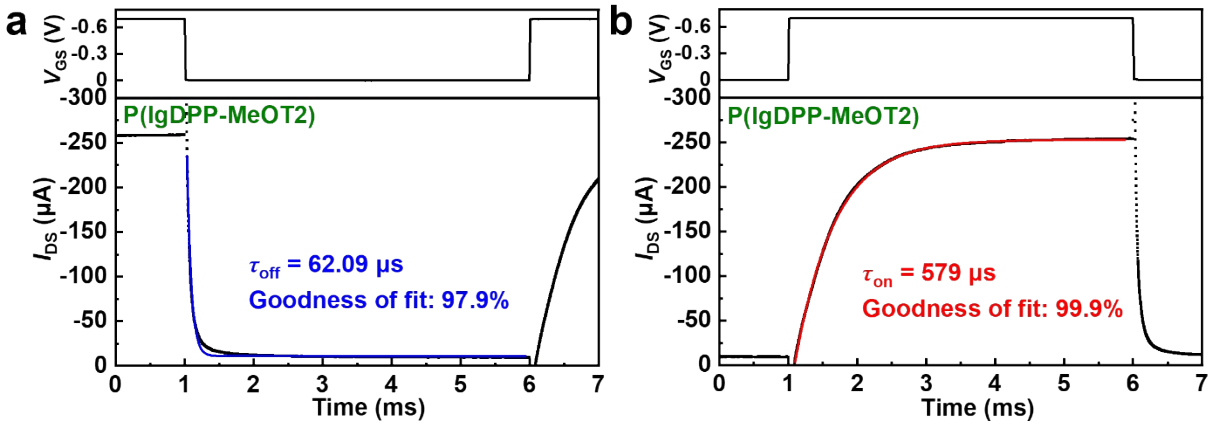

Figure S21 (a, b) Off- & on-time constant of P(lgDPP-MeOT2) obtained by applying a gate voltage pulse with a time scale of 5 ms. Blue and red lines were fitted through exponential decay function. W/L = 100/10 μm and d = 31.7±1.0 nm. V_{DS} was set to −0.6 V.

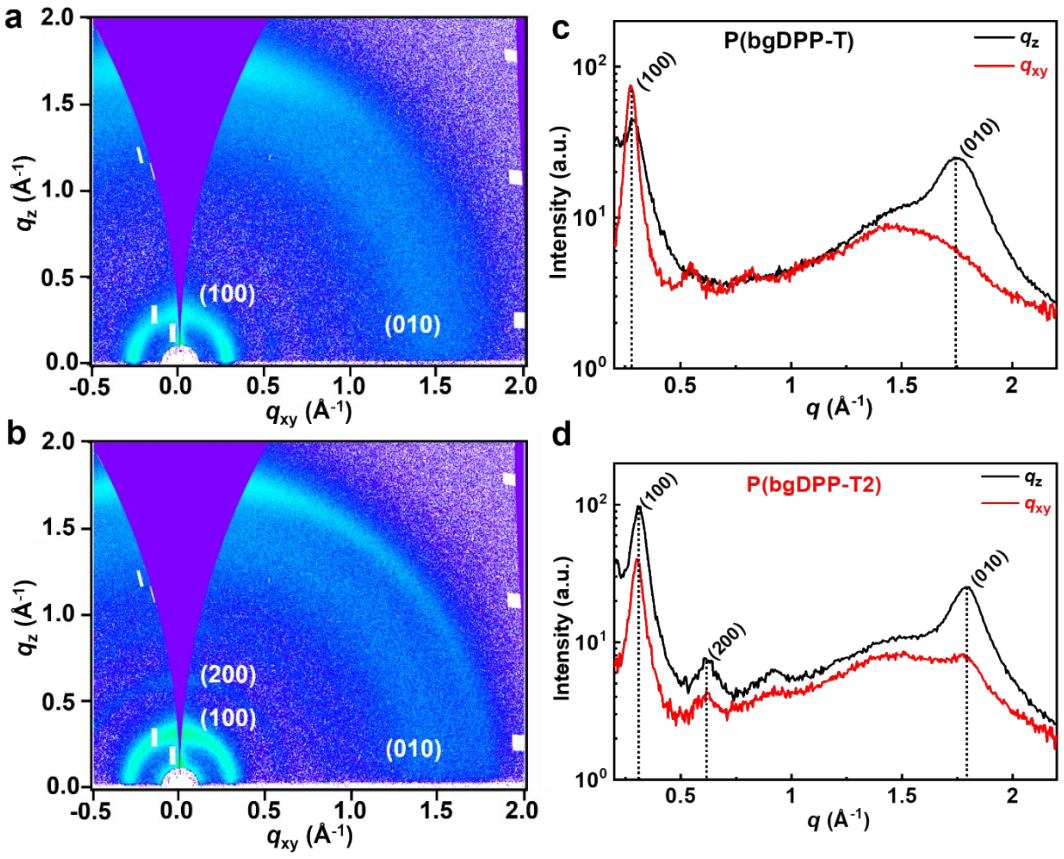

Figure S22 2D GIWAXS patterns of (a) P(bgDPP-T), and (b) P(bgDPP-T2). (c-d) The corresponding line cuts of P(bgDPP-T) and P(bgDPP-T2). Cuts along the q_{xy} direction (red) represent the scattering from the in-plane, while the scattering in the q_z direction (black) results from the out-of-plane. The associated lamellar (h00), and π-π stacking (0k0) peaks are indicated.

We also polymerized the linear glycol chain grafted DPP polymers with T and T2 donors, namely P(lgDPP-T) and P(lgDPP-T2), and we also measured the OECT performance of these two polymers. The chemical structure and the corresponding OECT performance of these two polymers are shown as below (Figure S23). The μC^* values of P(lgDPP-T) and P(lgDPP-T2) were measured as 10±2 $F \cdot cm^{-1} \cdot V^{-1} \cdot s^{-1}$ and 36±17 $F \cdot cm^{-1} \cdot V^{-1} \cdot s^{-1}$, respectively, which are smilar as P(bgDPP-T) and P(bgDPP-T2).

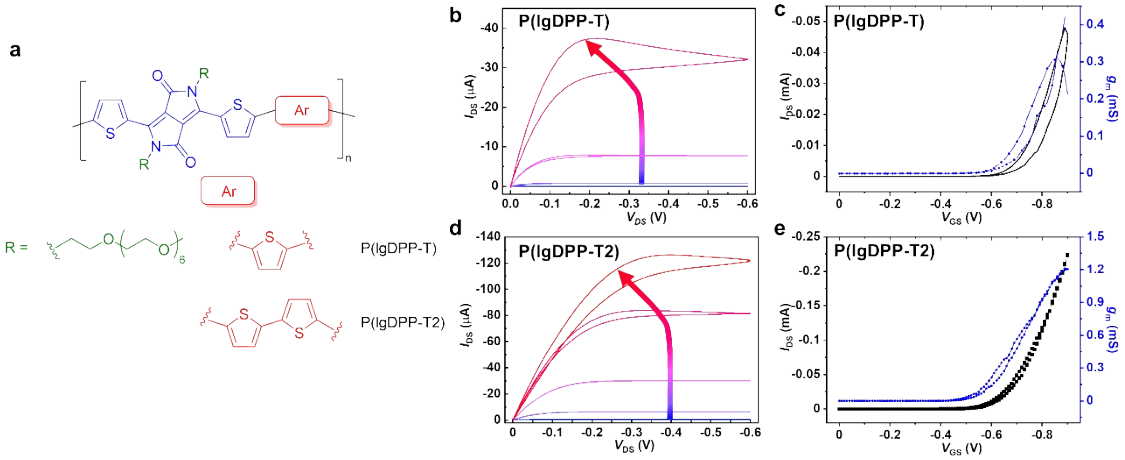

Figure S23 The output curves (b, d) and transfer curves (c, e) of OECT devices with P(lgDPP-T) and P(lgDPP-T2) (a) serving as the channel. Both polymers were dissolved with the solvent of HFIP as a concentration of 3 mg/ mL, and spin-casting with a rotating speed of 1000 rpm. The channel thickness was measured as 106.3±14.1 nm for P(lgDPP-T) and 72.2±20.4 nm for P(lgDPP-T2). W/L = 100-10 μm for all OECTs.

3. Synthetic Procedure and Characterization

Scheme S1. Synthesis of the monomers and polymers.

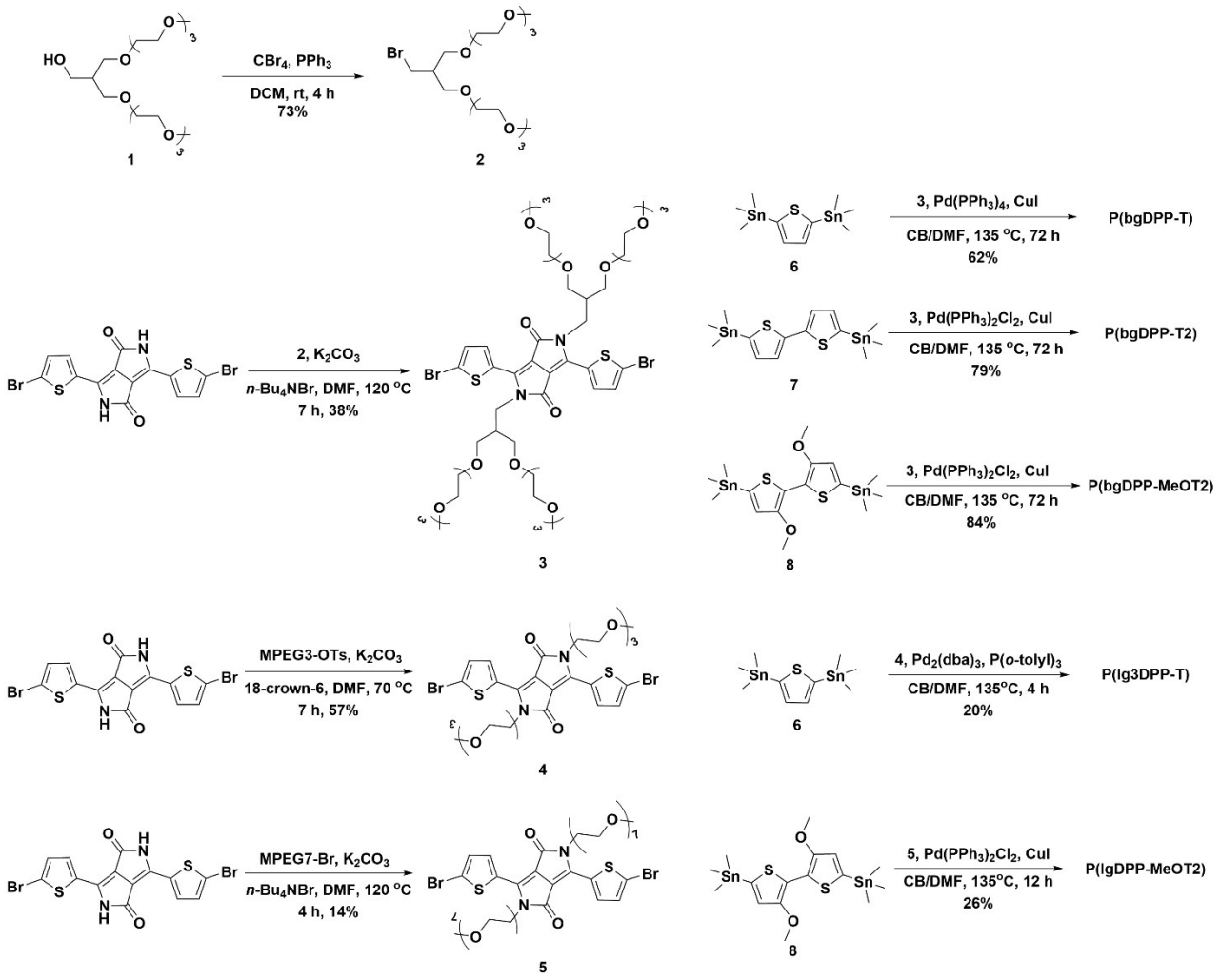

Compound **1** was synthesized according to the reported procedure.[14]

Synthesis of **2**: To a 25 mL two-necked round-bottom flask, **1** (500 mg, 1.26 mmol), carbon tetrabromide (461 mg, 1.39 mmol), and 5 mL DCM were added. Then triphenylphosphine (362 mg, 1.38 mmol) in 5 mL DCM was added slowly. The mixture was stirred at room temperature for 4 hours. The resulting mixture was sent to rotary evaporation, and the solvent was removed. The residue was purified through silica gel chromatography (DCM/ethyl acetate (EA) = 1/1) to afford **2** as a colorless liquid (425 mg, yield 73%). ^{1}H

NMR (400 MHz, $CDCl_3$) δ 3.68-3.45 (m, 30H), 3.39 (s, 6H), 2.27 (m, 1H). ^{13}C NMR (101 MHz, $CDCl_3$) δ 71.9, 70.6, 70.6, 70.5, 70.4, 70.0, 59.0, 41.3, 33.5. MALDI-TOF HRMS calcd. for $[M + NH_4]^+$: 461.1750; found: 461.1734.

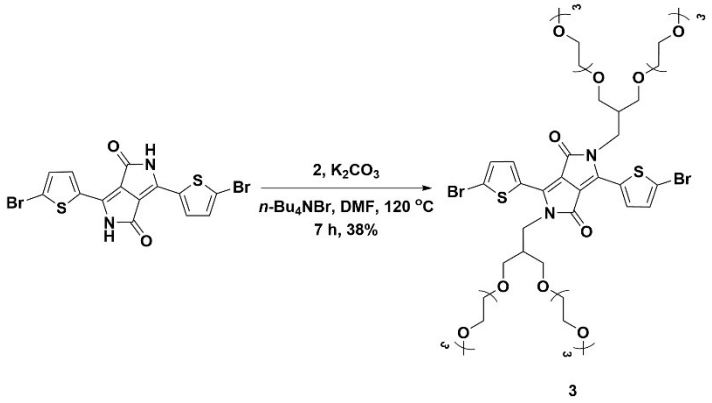

3

Synthesis of **3**: A 25 mL Schlenk tube was charged with **2** (440 mg, 0.95 mmol), 3,6-bis(5-bromothiophen-2-yl)-2,5-dihydropyrrolo[3,4-c]pyrrole-1,4-dione (DPP) (200 mg, 0.44 mmol), potassium carbonate (88 mg, 0.436 mmol), tetrabutylammonium bromide (300 mg, 0.93 mmol), and 5 mL dry DMF. The resulting mixture was heated to 120 °C and stirred for 7 h. Then the reaction mixture was cooled to room temperature and poured into water. The mixture was extracted with DCM with three times and washed with brine. Then the solvent was removed under reduced pressure, and the residue was purified by silica gel chromatography (DCM/methanol = 60/1) to afford **3** (201 mg, yield 38%) as a purplish red liquid. ^1H NMR (400 MHz, $CDCl_3$) δ 8.54 (d, J = 4.2 Hz, 2H), 7.22 (d, J = 4.2 Hz, 2H), 4.12 (d, J = 7.4 Hz, 4H), 3.63 (m, 56H), 3.36 (s, 12H), 2.43 (m, 2H). ^{13}C NMR (101 MHz, $CDCl_3$) δ 161.2, 134.7, 131.4, 131.2, 119.2, 107.7, 71.8, 70.6, 70.5, 70.4, 70.3, 70.0, 58.9, 41.6, 40.1. MALDI-TOF HRMS calcd. for $[M + NH_4]^+$: 1234.3396; found: 1234.3406.

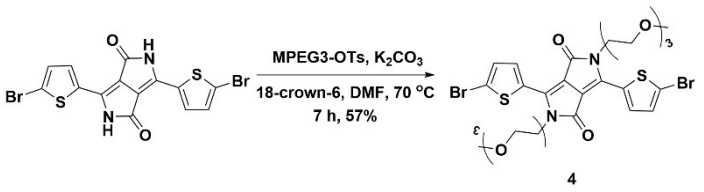

4

Synthesis of **4**: Under nitrogen atmosphere, to a 250 mL two-necked round-bottom flask, DPP (500 mg, 1.66 mmol), triethylene glycol monomethyl 4-methyl-benzenesulfonicacimethyl ester (MPEG3-OTs, 1.163 g, 3.66 mmol), potassium carbonate (176 mg, 1.66mmol), 18-crown-6 (5 mg, 0.02 mmol) and 30 mL anhydrous DMF were added. The mixture was heated and stirred under 70 °C for 8 hours. Then the mixture was poured

to water and exacted with DCM. The organic phase was dried with Na_2SO_4 and sent to a rotatary evaporator to remove the solvent. The residue was purified through silica chromatography (petroleum ether (PE)/EA = 3/1) to afford **4** as a dark red solid (574 mg, yield 57%). ^{1}H NMR (400 MHz, $CDCl_3$) δ 8.48 (d, J = 4.2 Hz, 2H), 7.20 (d, J = 4.2 Hz, 2H), 4.16 (t, J = 5.9 Hz, 4H), 3.77 (t, J = 5.9 Hz, 4H), 3.66–3.53 (m, 12H), 3.52–3.45 (m, 4H), 3.34 (s, 6H). ^{13}C NMR (101 MHz, $CDCl_3$) δ 161.2, 139.5, 134.8, 131.4, 131.1, 119.3, 107.9, 71.9, 70.8, 70.5, 70.5, 68.9, 59.0, 42.2. MALDI-TOF HRMS calcd. for $[M + NH_4]^+$: 766.0463; found: 766.0462.

Synthesis of ***5***

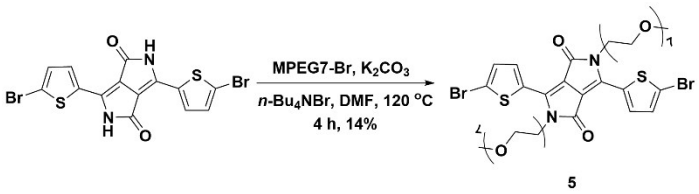

Under nitrogen atmosphere, to a 250 mL two-necked round-bottom flask, DPP (1.00 g, 2.18 mmol), methoxy hepta(ethylene glycol)bromide (MPEG7-Br, 1.101 g, 5.46 mmol), potassium carbonate (578 mg, 5.46 mmol), tetrabutylammonium bromide (1.40 g, 4.36 mmol), and 30 mL anhydrous DMF were added. The resulting mixture was heated to 120 ^{o}C and stirred for 4 h. Then the reaction mixture was cooled to room temperature and poured into water. The mixture was extracted with DCM three times and washed with brine. Then the solvent was removed under reduced pressure, the residue was purified by silica gel chromatography (DCM/methanol = 40/1) to afford **5** (351 mg, yield 14%) as a purplish-red solid. ^{1}H NMR (400 MHz, $CDCl_3$) δ 8.46 (d, J = 4.2 Hz, 2H), 7.18 (d, J = 4.2 Hz, 2H), 4.14 (t, J = 5.9 Hz, 4H), 3.74 (t, J = 5.9 Hz, 4H), 3.67-3.49 (m, 48H), 3.35 (s, 6H). ^{13}C NMR (101 MHz, $CDCl_3$) δ 161.1, 134.8, 131.3, 131.0, 119.2, 107.9, 70.7, 70.5, 70.5, 70.4, 68.8, 58.9, 42.1. MALDI-TOF HRMS calcd. for $[M+ NH_4]^+$: 1118.2559; found: 1118.2559.

General Procedure for Polymerization:

To a 25 mL Schlenk tube, tin reagent (1.00 eq.), DPP monmer (1.00 eq.), Pd catalyst (0.04 eq.), CuI (0.04 eq.), anhydrous DMF, and anhydrous chlorobenzene were added under nitrogen atmosphere. The tube was charged with nitrogen through a *freeze-pump-thaw* cycle for three times. The sealed tube was heated to 135 ^{o}C and stirred for a given time (Scheme S1). After cooling the reaction mixture to room temperature, diethylphenylazothioformamide (3 mg) was added to remove the catalyst and the resulting mixture was

stirred at 80 °C for 1 h. The reaction mixture was poured into 20 mL hexane to precipitate the polymer and filtered. The polymer solid was placed in a Soxhlet extractor and extracted with hexane, methanol, acetone, and chloroform. The chloroform solution was concentrated under reduced pressure and then poured into 20 mL hexane to re-precipitate the polymer. The suspension was filtered and dried in vacuum to afford the polymer.

P(lg3DPP-T): Dark green solid (yield: 20%). Most of the polymer is insoluble, leading to a low yield.

P(bgDPP-T): Dark green solid (yield: 62%). ^{1}H NMR (600 MHz, $CDCl_3$, 293 K, ppm) δ 8.83, 7.73, 4.24, 3.84-3.45, 3.35, 2.45.

P(bgDPP-T2): Dark green solid (yield: 79%). ^{1}H NMR (600 MHz, $CDCl_3$, 293 K, ppm) δ 8.84, 7.05, 4.22, 3.78-3.55, 3.35, 2.52.

P(bgDPP-MeOT2): Dark green solid (yield: 84%). ^{1}H NMR (400 MHz, $CDCl_3$, 293 K, ppm) δ 8.90, 7.12, 4.04, 3.95–3.45, 3.35, 2.52.

P(lgDPP-MeOT2): Dark green solid (yield 26%). Most of the polymer is insoluble, leading to a low yield. ^{1}H NMR (500 MHz, $CDCl_2CDCl_2$, 383 K, ppm) δ 8.81, 7.37, 7.15, 4.43-3.43, 3.20.

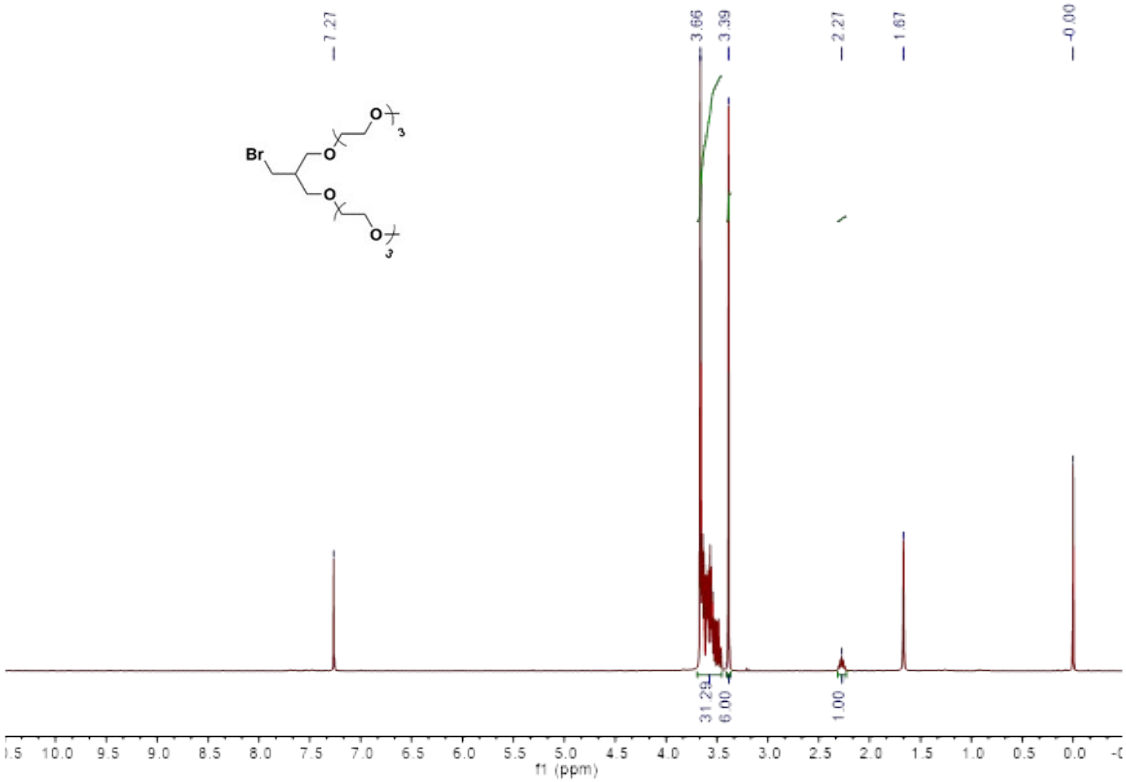

4. ^{1}H and ^{13}C NMR spectra

Figure S24 ^{1}H NMR spectrum of **2**.

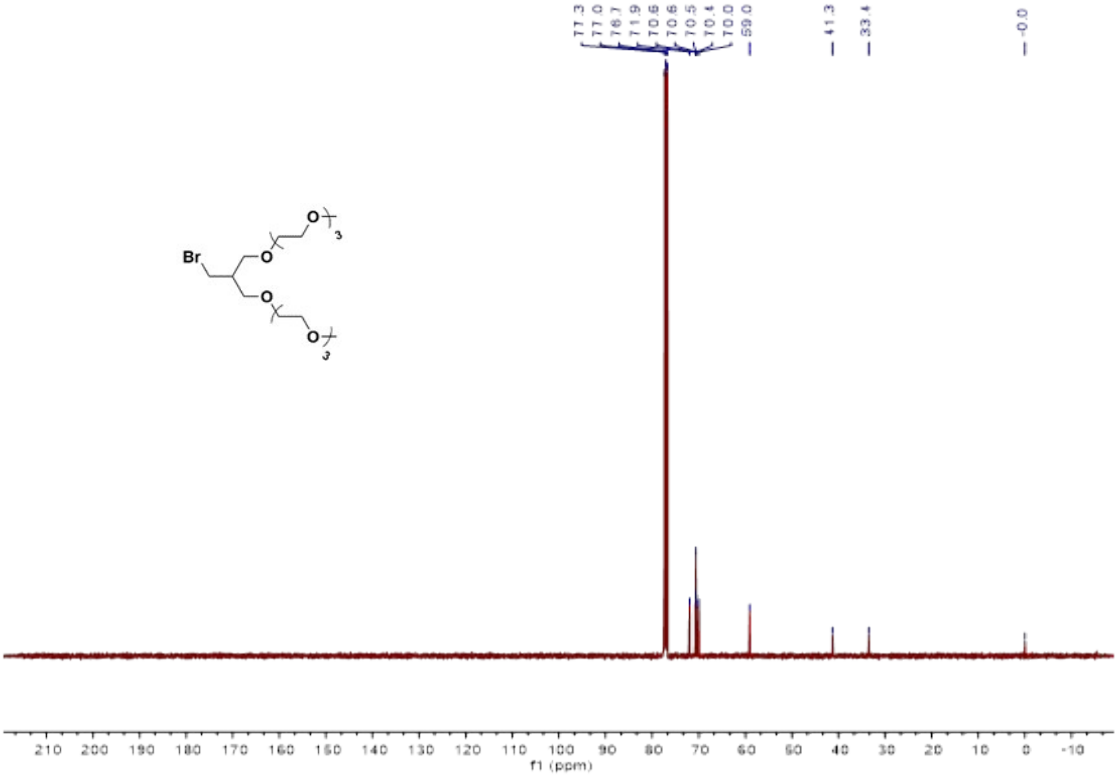

Figure S25 ^{13}C NMR spectrum of **2**.

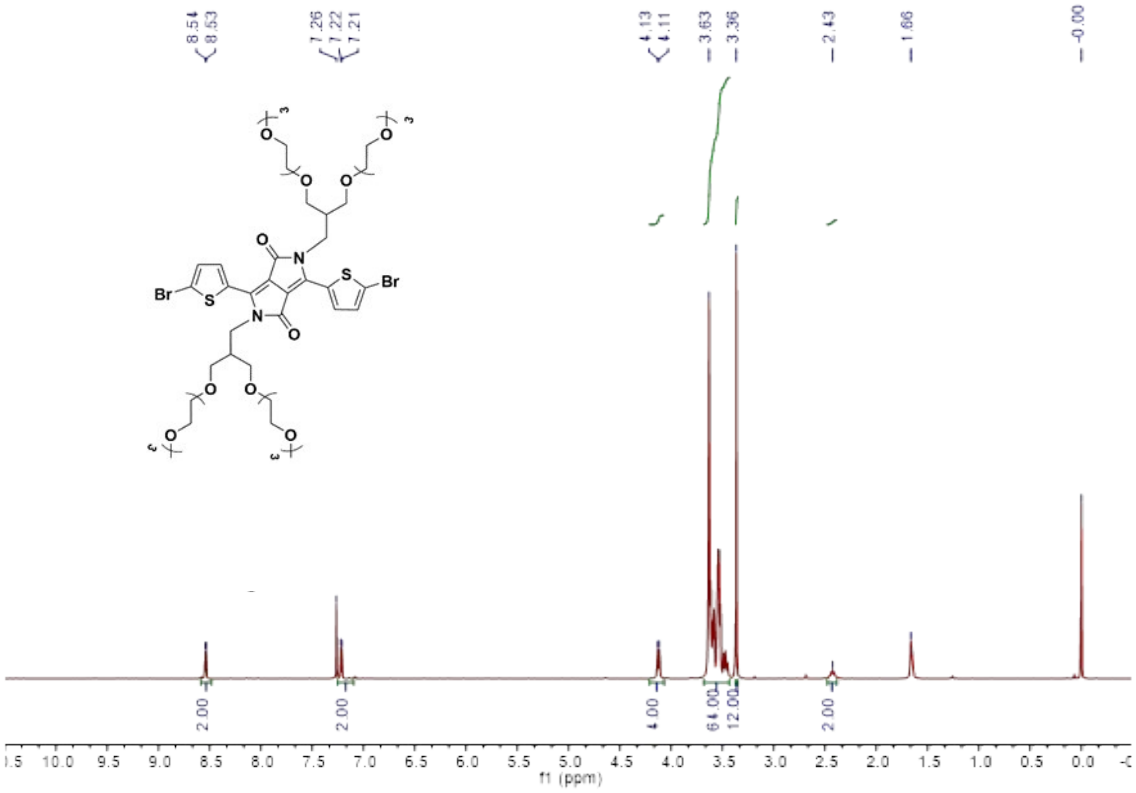

Figure S26 ^{1}H NMR spectrum of **3**.

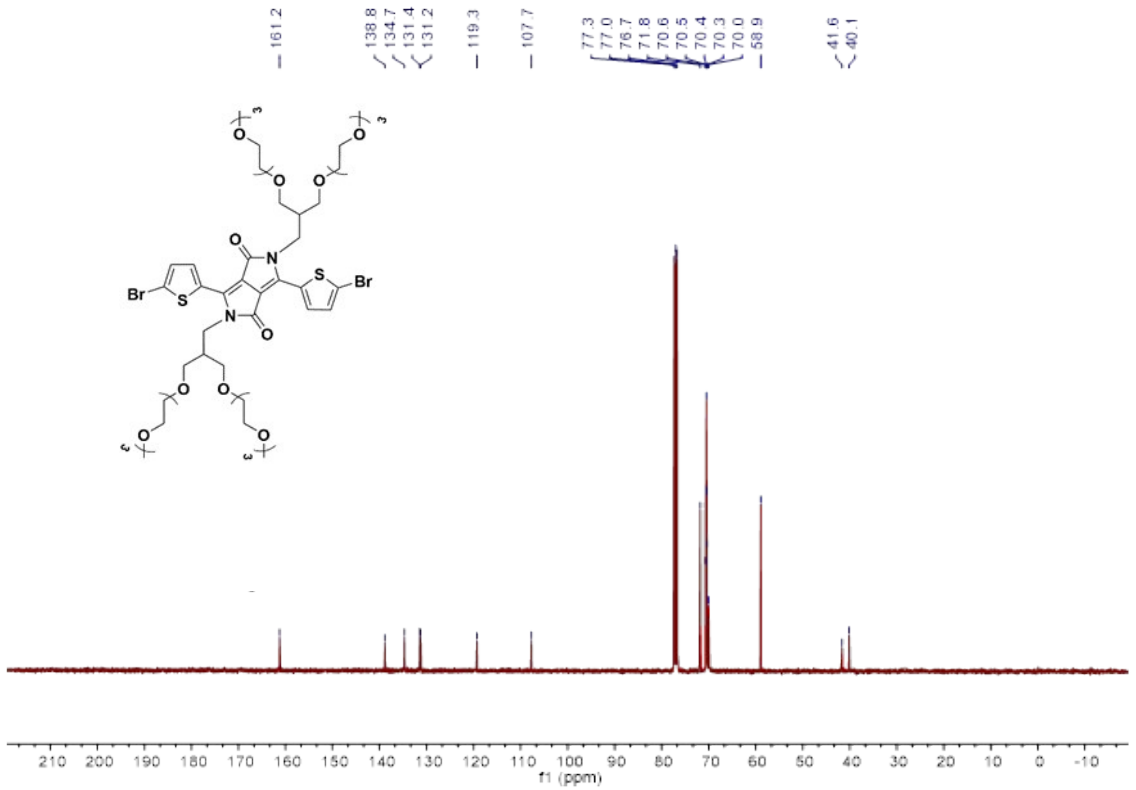

Figure S27 ^{13}C NMR spectrum of **3**.

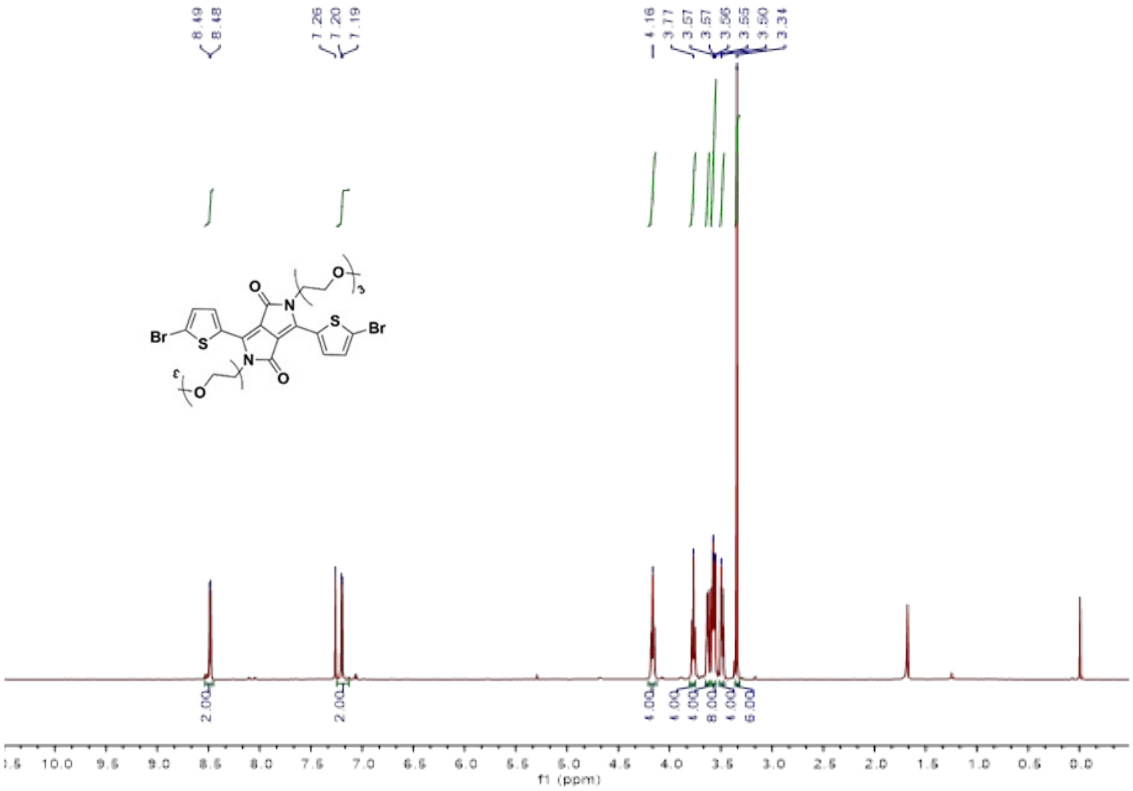

Figure S28 ^{1}H NMR spectrum of **4**.

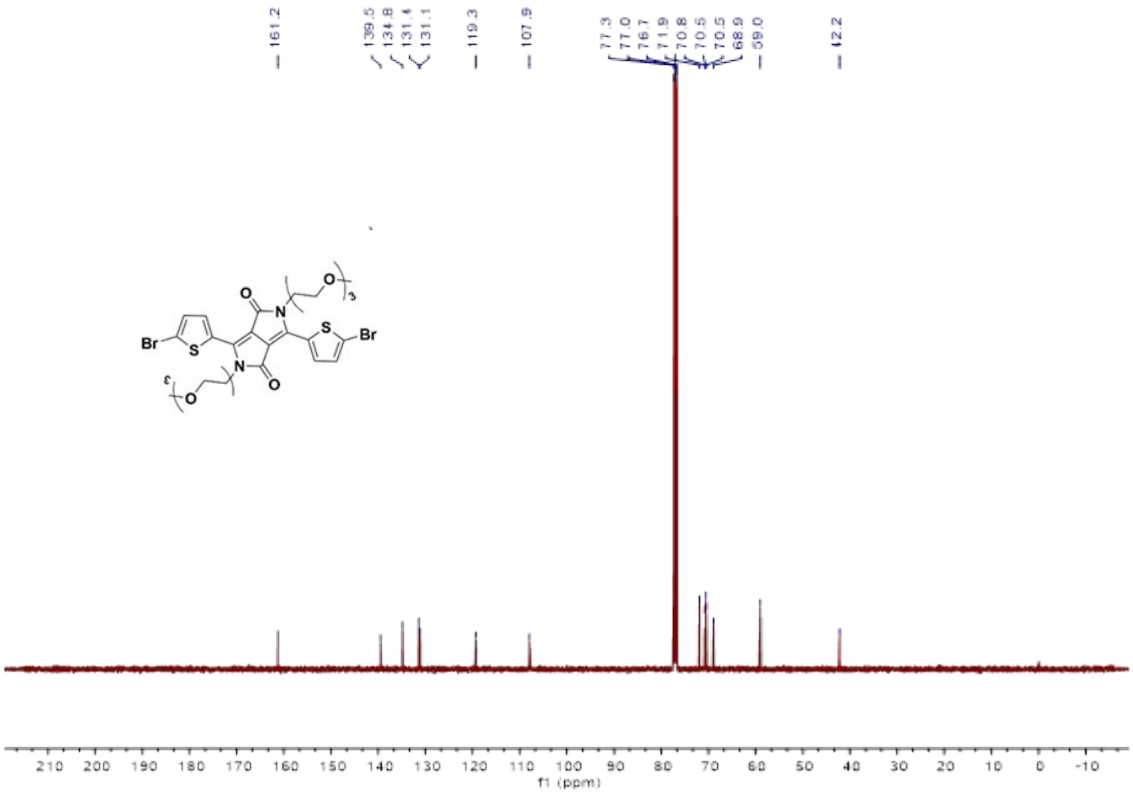

Figure S29 ^{13}C NMR spectrum of **4**.

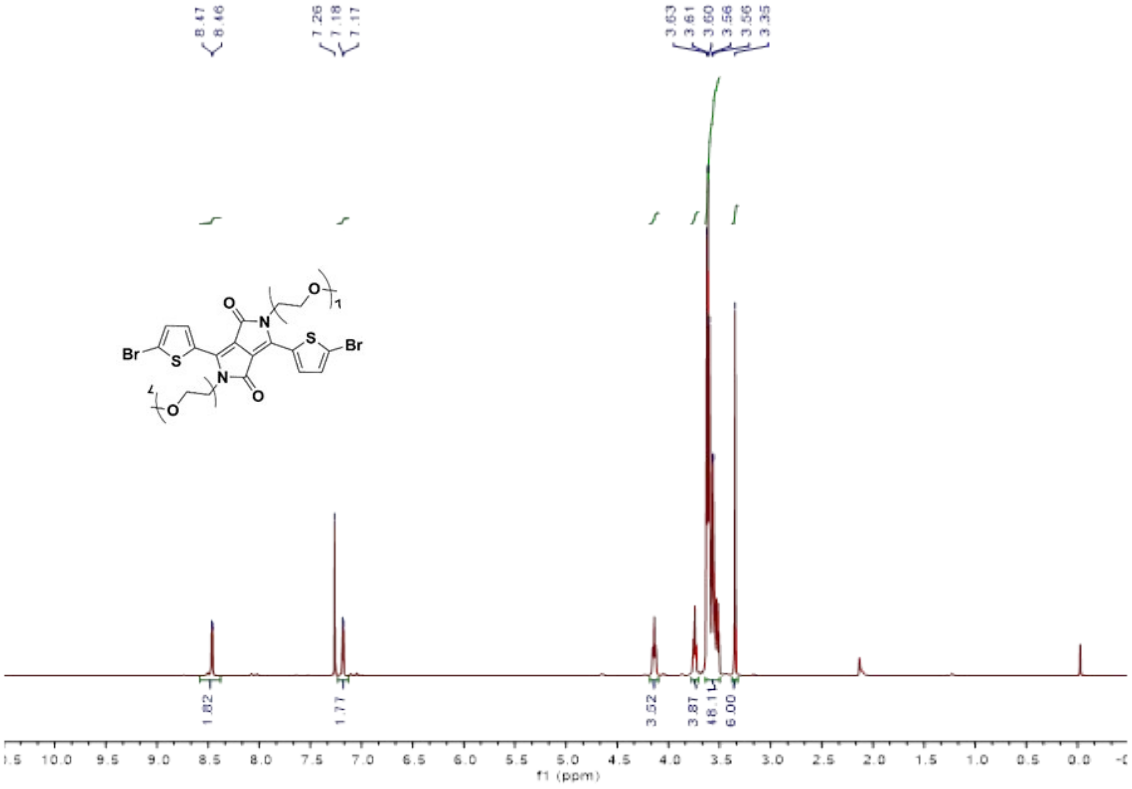

Figure S30 ^{1}H NMR spectrum of **5**.

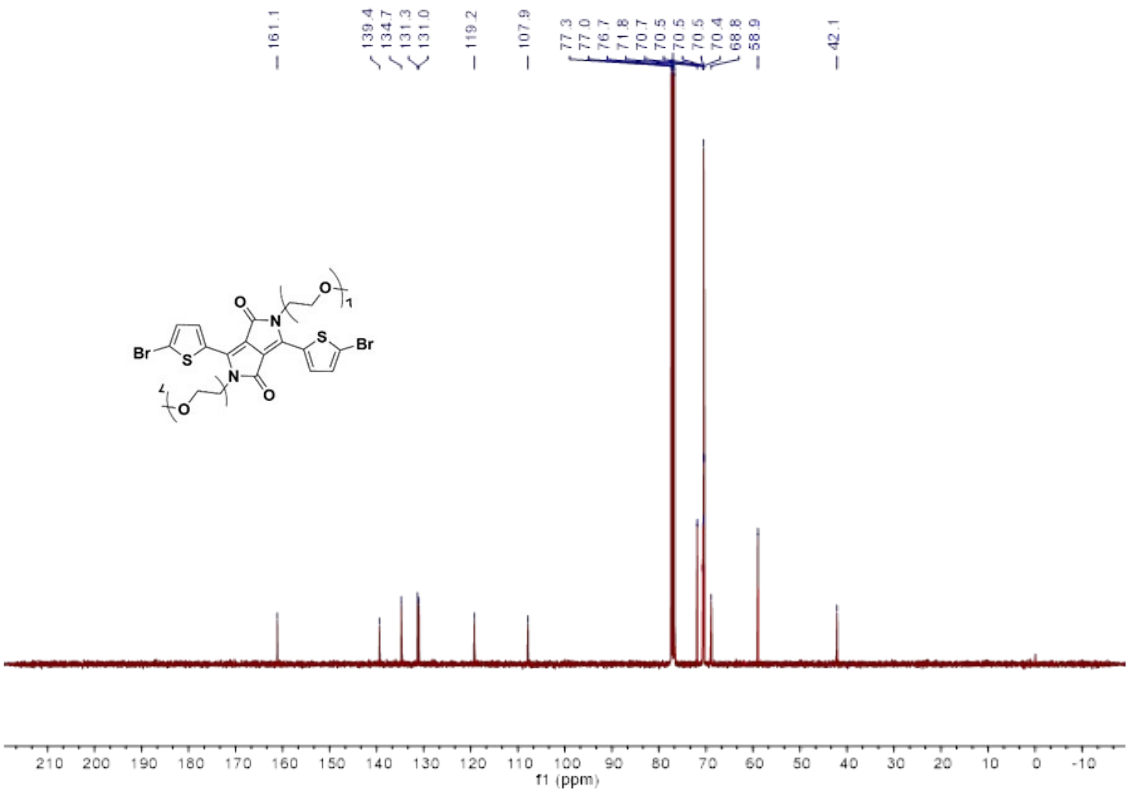

Figure S31 ^{13}C NMR spectrum of **5**.

5. References:

1 J. Qiu, T. Yu, W. Zhang, Z. Zhao, Y. Zhang, G. Ye, Y. Zhao, X. Du, X. Liu, L. Yang, L. Zhang, S. Qi, Q. Tan, X. Guo, G. Li, S. Guo, H. Sun, D. Wei and N. Liu, *ACS Materials Letters*, 2020, **2**, 999.

2 C. B. Nielsen, A. Giovannitti, D. T. Sbircea, E. Bandiello, M. R. Niazi, D. A. Hanifi, M. Sessolo, A. Amassian, G. G. Malliaras, J. Rivnay and I. McCulloch, *J. Am. Chem. Soc.*, 2016, **138**, 10252.

3 M. Moser, L. R. Savagian, A. Savva, M. Matta, J. F. Ponder, T. C. Hidalgo, D. Ohayon, R. Hallani, M. Reisjalali, A. Troisi, A. Wadsworth, J. R. Reynolds, S. Inal and I. McCulloch, *Chem. Mater.*, 2020, **32**, 6618.

4 A. Giovannitti, D. T. Sbircea, S. Inal, C. B. Nielsen, E. Bandiello, D. A. Hanifi, M. Sessolo, G. G. Malliaras, I. McCulloch and J. Rivnay, *Proc. Natl. Acad. Sci. U. S. A.*, 2016, **113**, 12017.

5 A. Savva, R. Hallani, C. Cendra, J. Surgailis, T. C. Hidalgo, S. Wustoni, R. Sheelamanthula, X. Chen, M. Kirkus, A. Giovannitti, A. Salleo, I. McCulloch and S. Inal, *Adv. Funct. Mater.*, 2020, **30**, 1907657.

6 M. Moser, T. C. Hidalgo, J. Surgailis, J. Gladisch, S. Ghosh, R. Sheelamanthula, Q. Thiburce, A. Giovannitti, A. Salleo, N. Gasparini, A. Wadsworth, I. Zozoulenko, M. Berggren, E. Stavrinidou, S. Inal and I. McCulloch, *Adv. Mater.*, 2020, DOI: 10.1002/adma.202002748, e2002748.

7 D. Khodagholy, J. Rivnay, M. Sessolo, M. Gurfinkel, P. Leleux, L. H. Jimison, E. Stavrinidou, T. Herve, S. Sanaur, R. M. Owens and G. G. Malliaras, *Nat. Commun.*, 2013, **4**, 2133.

8 S. Inal, J. Rivnay, P. Leleux, M. Ferro, M. Ramuz, J. C. Brendel, M. M. Schmidt, M. Thelakkat and G. G. Malliaras, *Adv. Mater.*, 2014, **26**, 7450.

9 S. Inal, G. G. Malliaras and J. Rivnay, *Nat. Commun.*, 2017, **8**, 1767.

10 Y. Wang, E. Zeglio, H. Liao, J. Xu, F. Liu, Z. Li, I. P. Maria, D. Mawad, A. Herland, I. McCulloch and W. Yue, *Chem. Mater.*, 2019, **31**, 9797.

11 H. Sun, M. Vagin, S. Wang, X. Crispin, R. Forchheimer, M. Berggren and S. Fabiano, *Adv. Mater.*, 2018, **30**, 1704916.

12 A. T. Lill, D. X. Cao, M. Schrock, J. Vollbrecht, J. Huang, T. Nguyen-Dang, V. V. Brus, B. Yurash, D. Leifert, G. C. Bazan and T. Q. Nguyen, *Adv. Mater.*, 2020, DOI: 10.1002/adma.201908120, e1908120.

13 A. Giovannitti, R. B. Rashid, Q. Thiburce, B. D. Paulsen, C. Cendra, K. Thorley, D. Moia, J. T. Mefford, D. Hanifi, D. Weiyuan, M. Moser, A. Salleo, J. Nelson, I. McCulloch and J. Rivnay, *Adv. Mater.*, 2020, **32**, e1908047.

14 J. Buendia and L. Sanchez, *Org. Lett.*, 2013, **15**, 5746.